FUDMA Journal of Sciences (FJS)
ISSN online: 2616-1370
ISSN print: 2645 - 2944
Vol. 10 No. 6, March, 2026, pp 314 – 320
DOI: https://doi.org/10.33003/fjs-2026-1006-5172

GROWTH AND CHARACTERIZATION OF INDIUM OXIDE MICROSTRUCTURES USING CHEMICAL VAPOUR DEPOSITION METHOD

[*1]Aper, M. Terwase, [1]Ikyumbur, T. Jonathan, [2,3]McAsule, A. Augustine, [1]Amon, S. Paul and [3,4]Obaseki, S. Oluwatosin

[1]Department of Physics, Rev.Fr. Moses Orshio Adasu University, P. M. B. 102119, Makurdi, Nigeria.
[2]Department of Industrial Physics, Joseph Sarwuan Tarka University, P.M.B. 2373 Makurdi, Nigeria.
[3]School of Physics, Universiti Sains Malaysia, 11800 Penang, Malaysia.
[4]Department of Physical Sciences, Landmark University, PMB 1001 Omu-Aran, Kwara State, Nigeria.

*Corresponding authors' email: taper@bsum.edu.ng

ABSTRACT

Indium oxide (In_2O_3) thin films are typically deposited on quartz, sapphire, and silicon substrates by chemical vapour deposition (CVD) because of the high temperatures required during film growth. In this study, however, high-quality In_2O_3 thin films were successfully deposited on glass substrates using the CVD technique. The source temperature was varied from 850 °C to 1000 °C, while the substrates were positioned downstream in a lower-temperature region maintained between 400 °C and 500 °C. The morphological, structural, and optical properties of the deposited films were characterized using field-emission scanning electron microscopy (FESEM), X-ray diffraction (XRD), and UV–Visible spectrometry, respectively. The results revealed significant temperature-dependent changes in the film morphology, accompanied by improved crystallinity at higher deposition temperatures. Optical studies further showed a reduction in the optical bandgap from 3.470 eV to 3.021 eV with increasing growth temperature. These findings demonstrate that controlled downstream CVD growth provides an effective route for synthesizing crystalline In_2O_3 thin films on low-cost glass substrates with tunable optical properties.

Keywords: Indium Oxide, Thin film, Microstructures, Nanostructures, Bandgap energy

INTRODUCTION

Indium oxide is a semiconductor metal oxide material that has been studied by many in the recent past decades for a number of applications. It is an important ingredient especially in the production of photovoltaic, optoelectronics, photoelectrochemical, and nanoelectronics devices (Gan et al., 2013; Karazhanov et al., 2007; Chao Li et al., 2003; Conan Li & Han, 2003; Mahalingam & Abdullah, 2016; Qurashi et al., 2010). Indium oxide earned its importance from its unique properties such as, wide energy band gap, high electrical conductivity and electron mobility, and high optical transmittances as well as chemical stability (King et al., 2009; Lei et al., 2014a; Piper et al., 2009). Thin film indium oxide has been investigated for advanced technological applications including waveguides, field-effect transistors, and transparent thin film transistors. The functionality of most devices of In_2O_3 thin films is said to be influenced by their morphologies. For instance, nanoparticle for toxic gas sensing, nanowires for optoelectronics, efficient field emission, chemical sensing, single-crystalline In_2O_3 pyramids for efficient field emission, etc (Domènech-Gil et al., 2017; Her & Chang, 2017; Karn et al., 2017; C. Li et al., 2003; Ma et al., 2018; Zhang et al., 2020).

Different synthesis methods have been used to prepare In_2O_3 thin films including, sol-gel spin coating, magnetron sputtering, spray pyrolysis, chemical vapour deposition (CVD), and many others (Aper et al., 2023; Hosseini et al., 2013). Based on the preparation technique, the precursors, the substrates, and the growth conditions, In_2O_3 thin films of varying properties have been reported by many over the years. Commonly, quartz, sapphire, and silicon based substrates are used in preparing In_2O_3 films by the CVD method largely because of the high deposition temperature in the reaction chamber (T M Aper et al., 2021; Lei et al., 2014b; Stroescu et al., 2013; Yahia et al., 2019). In this work however, we report the growth of In_2O_3 thin films on glass substrate via the CVD technique. This has been possible by carefully studying the downstream temperature where glass can withstand and material growth achievable. Variation in the source temperature reveals visible transformations in the properties of the synthesized films.

MATERIALS AND METHODS

Experimental Setup

Synthesis of the In_2O_3 microstructured films in this work was carried out by the chemical vapour deposition technique under atmospheric pressure using a CVD CARBOLITE model system. Figure 1 is a schematic representative of the experimental setup for the CVD synthesis of the In_2O_3 films. The system consists of a microprocessor-controlled central heating horizontal tube furnace with a maximum heating capacity of 1200 ^oC. The furnace was fitted with a quartz tube of 4.60 cm and 5.00 cm, inner and outer diameter respectively, and a length of 125.00 cm. From the central heating zone, the furnace's temperature on both sides decreases as you move away from it. Stainless steel couplers were connected at both ends of the tube. The downstream end was connected to the exhaust, while the upstream end was connected to the mass flow meter. A desired flow rate of the purging gas was delivered directly into the reaction chamber through the gas inlet, while the carrier/forming gas was either let in directly or pass through a vapour reservoir that was placed upstream containing deionized (DI) water at an elevated temperature (about 70 ^oC).

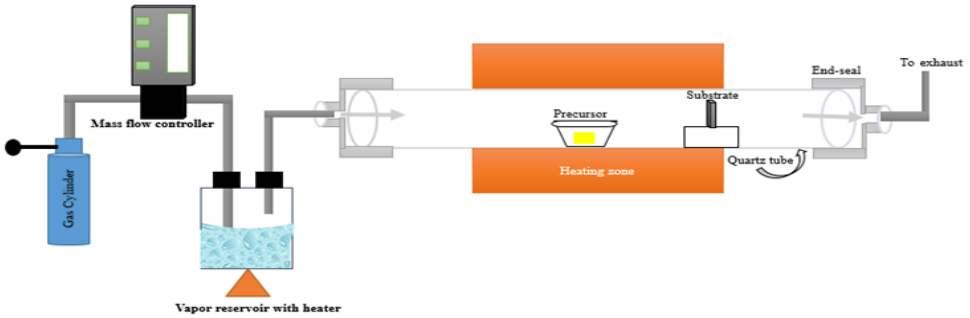

Figure 1: Schematic Representation of the Experimental Setup for the CVD Deposition of the In_2O_3 Films

Materials and the Deposition Procedure

In this study, In_2O_3 films were synthesized by the CVD technique using a mixture of indium oxide powder and graphite as precursor and reducing agent respectively. The carrier gas was a 1 % hydrogen balance nitrogen gas (H_2/N_2) which was delivered into the reaction chamber through vapour reservoir as explained in the above section. A microscope glass slide was used as the substrate. The glass slide was cut into 1 cm ×1 cm pieces, and ultrasonically cleared in a 20 % Decon 90 solution for 15 minutes followed by three sonicated rinsing with deionized water for five minutes each. The substrates were then oven dried at 120ºC for 20 minutes and finally blown with nitrogen gum. After heating the reaction chamber to the initial deposition temperature of 850 ºC, the source material was taken in a ceramic boat and position at the central heating zone, while the substrate was placed vertically at a distance of about 27 cm downstream from the central heating point, at a height of about 3 cm from the horizontal plane of the quartz tube. 50 sccm of H_2/N_2 gas was then fed in from the upstream through a bubbler containing DI water at elevated temperature of 75 ºC. After 60 min of deposition, the system was switched off and allow to cool down for 60 min before removing the sample. To investigate the influence of deposition temperature on the properties of the films, three more samples were grown at 900, 950 and 1000 ºC while keeping the other parameters constant.

The synthesized films were analyzed for morphological and elemental composition, structural and optical properties using FEI Nova NanoSEM 450 field emission scanning electron microscope (FE-SEM), PANanalytical X' pert PRO high-resolution X-ray diffraction (HR-XRD) instrument with Cu K_α (λ=0.15405 nm) radiation source and ultraviolet-visible near-infrared spectrophotometer (UV-vis-NIR) Agilent Cary 5000 instruments respectively.

Morphological Analysis

The surface images of the synthesized films are given in figure 2. G-850, G-900, G-950, and G-1000 represents samples grown at 850, 900, 950, and 1000 ºC respectively. The FESEM images revealed the formation of micro-crumbs-like structures and micro-wires interconnecting with the micro-crumbs for the growth at 850 ºC. Interconnecting rods having rough surface can be observed for the sample synthesized at 900 ºC. Increased deposition temperature led to the formation of micro-blocks of varying sizes for the synthesis at 950 and 1000 ºC. The observed changes in the surface morphology of the developed films can be ascribed to the increased substrate temperature due to increase in the growth temperature. Enhanced process temperature will also improve the rate of vaporization of the source material and hence increase material growth.

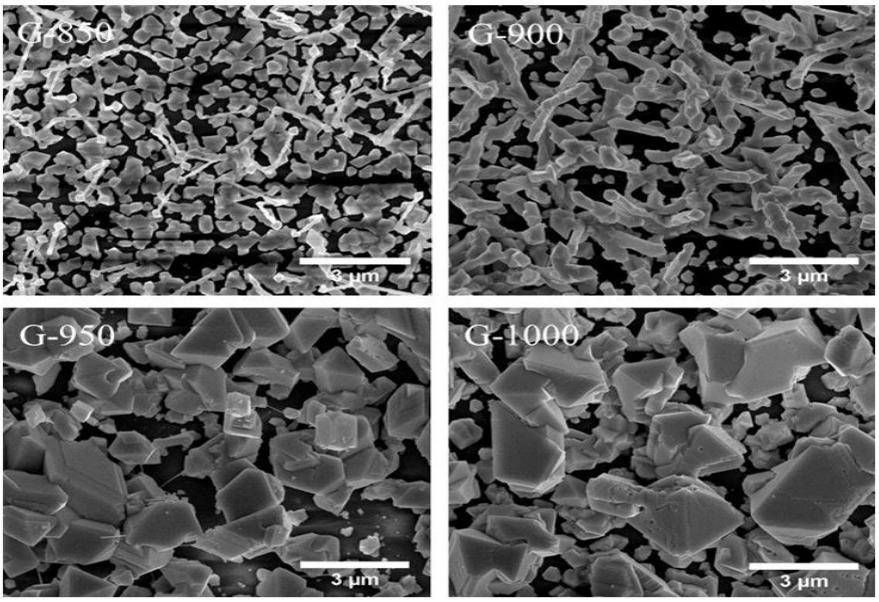

Figure 2: FESEM Images for In_2O_3 Films Synthesized on Glass Substrates at Various Deposition Temperature

Elemental Composition

The EDX spectra of the In_2O_3 films prepared at different source temperatures are given in Figure 3. The chemical composition of In and O phases were identified in all the samples. In addition to the observed In and O phases, other peaks of Na, Mg, Si, and Ca that may be due the substrate material (glass) were also identify especially for sample G-850 (deposited at 850 ^oC). These peaks however, decreases with increased deposition temperature and no signals were recorded from them at the higher growth temperatures. This indicates increase density of material growth due to enhanced evaporation of the precursor at higher deposition temperature. Figure 4 shows a variation in In/O atomic ratio of the sample with increased deposition temperature. The figure revealed increased In/O ratio from sub-stoichiometric at lower deposition temperatures to values greater than the stoichiometric value (0.667) at higher growth temperatures. High stoichiometric value indicates oxygen deficiency in the samples.

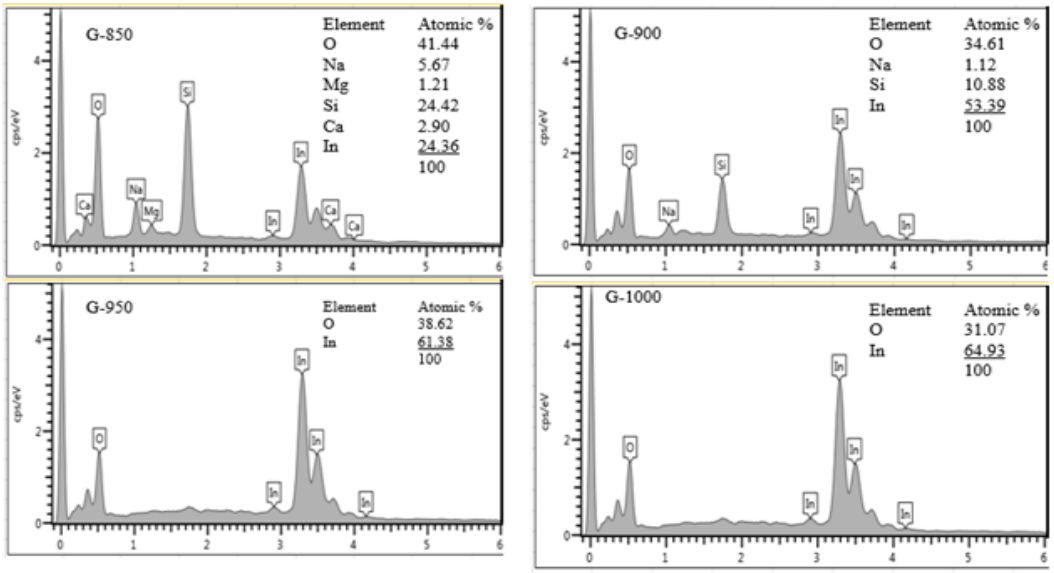

Figure 3: EXD Elemental Composition Spectra of the In_2O_3 Films Deposited on Glass Substrates at Different Growth Temperatures

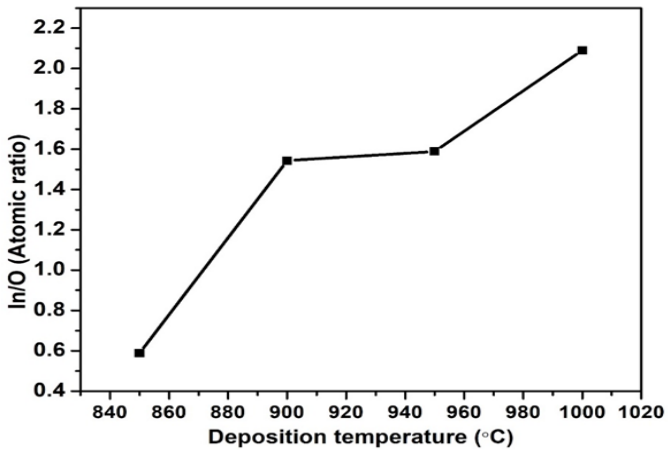

Figure 4: Variation of in/O Atomic Ratio with Growth Temperature of the In_2O_3 Films

Structural Characterization

Figure 5 depicts the XRD spectra for the In_2O_3 films fabricated at different temperatures. The XRD measurement was taken by performing a continuous Gonio scan of 2θ in the range between 20 and 80 ^{o} at a step size of 0.05 (^{o} 2θ) and scan step time of 1.5 (s). The samples can be seen to exhibit a strong diffraction peak at about 2θ = 30.54 ^{o} corresponding to the (222) crystallographic plane of the body centred cubic (bcc) structure of the In_2O_3 (JCPDS 00-044-1087). Other minor peaks could also be observed at about 35, 37, 41, 45, 60, and 63 ^{o} respectively corresponding to the (400), (332), (431), (440), (622), and (444) planes of the cubic In_2O_3 crystal structure. The multiple diffraction peaks confirm the formation of polycrystalline material. The intensity of the peaks can be seen to first enhanced with deposition temperature, then decreased for the deposition at 950 ^oC, and finally increased for the growth at 1000 ^oC. The observed variation in the diffraction peaks intensity could be ascribed to increase in material growth and enhanced crystallinity. It may also be related to surface transformation in the synthesized material as can be seen in the FESEM images.

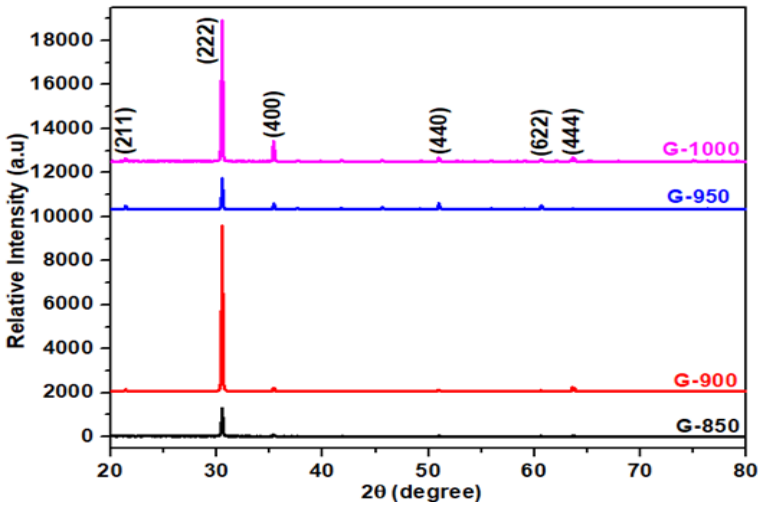

Figure 5: XRD Patterns of In_2O_3 Thin Films Deposited at Different Temperatures

Peak profile analysis was carried out on the most intense peak in the samples. Using the Bragg's law Eq. (1) (Ray et al., 1983; Sakaliuniene et al., 2011),

$$n\lambda = 2dSin\theta \quad (1)$$

where $n = 1$ is the first diffraction order, λ is the X-ray wavelength and d is the separation between the planes of a given miller indices h, k, l. From Eq. (1), d-spacing can be written as Eq. (2). In the In_2O_3 cubic structure, the lattice constants a=b=c such that, the d-spacing is related to the miller indices by Eq. (3).

$$d = \frac{\lambda}{2Sin\theta} \quad (2)$$

$$a = \frac{d_{hkl}}{\sqrt{h^2 + k^2 + l^2}} \quad (3)$$

The interplanar spacing and the lattice constant values obtained from the (222) plane of the XRD data for the In_2O_3 films synthesized at different deposition temperatures are consistent with the reference (JCPDS 00-044-1087) data of In_2O_3. The sample's percentage variation of the d-spacing values is given in Table 1.

Table 1: Related Structural Parameters Obtained from the Dominate (222) Diffraction Peak of the In_2O_3 Microstructures

Sample	Observed 2θ (º)	d_{ref} (Å)	d_{ref} (Å)	% deviation in d
G-850	30.536		2.925	0.137
G-900	30.532	2.921	2.926	0.171
G-950	30.540		2.925	0.137
G-1000	30.526		2.926	0.171

In XRD data characterization, peak profile analysis is performed to determine the peak broadening with crystallite size and lattice strain due to deformation. The highest intensity in the (222) diffraction peak of the synthesized films indicates that, the grown In_2O_3 microstructures have a preferential crystallographic (222) orientation. The Debye-Scherrer expression, Eq. (4) (Jubu et al., n.d.) was used to calculate the average crystallite size from the XRD peak width of the (222) plane. The strain of the films indicating peak broadening due to crystal imperfection and dislocation on the other hand was estimated using Eq. (5).

$$D = \frac{K\lambda}{\beta \cos\theta} \quad (4)$$

$$\varepsilon = \frac{\beta \cos\theta}{4} \quad (5)$$

where D is the crystallite size, K is a constant (K=0.9), β is the FWHM, ε is the strain, λ is the wavelength of the X-ray source, and θ is the Bragg angle. Summary of D full width at half-maximum (FWHM), and ε for the films as obtained from their XRD data are given in Table 2.

Table 2: Summary of D, FWHM, and ε Obtained from the Dominate (222) Diffraction Peak of the In_2O_3 Microstructures

Sample	Observed 2θ (º)	FWHM	D (nm)	ε ×10^{-3}
G-850	30.536	0.1214	65.833	1.941
G-900	30.532	0.1052	78.278	1.682
G-950	30.540	0.1116	73.791	1.784
G-1000	30.526	0.1099	74.929	1.757

Optical Bandgap of the In_2O_3 Films

Diffuse reflectance measurement was performed to determine the optical bandgap of the In_2O_3 samples synthesized at various temperatures. Figure 6(a), represents the reflectance spectra for the samples in an incident photon wavelength range of 250-800 (nm). The spectra show low reflectance in all the films with a sharp absorption edge. A shift in the absorption edge to larger angles and marginal increase in reflectance with increase in the deposition temperature can be observed in the curves. This may be related to the changes in the materials' particle size and surface transformation.

The optical band gap of a semiconductor describes the energy required to excite an electron from the valence band to the conduction band. A correct determination of the band gap energy is essential in predicting the photochemical and photophysical properties of semiconductors. The band gap energy is of particular importance when discussing the photocatalytic properties of semiconductor materials. According to Tauc theory, the band gap values of semiconductors can be determined from the optical absorption spectra. This method assumed that the energy-dependent absorption coefficient (α) can be expressed as in Eq. (6) (Ahmed et al., 2019; Elam et al., 2006; Liang et al., 2001),

$$(\alpha h\nu) = C(h\nu - E_g)^n \quad (6)$$

where h is the Planck constant, ν is the frequency of incident photon, C is a constant, E_g is the material average band gap energy and n is a factor which depends on the type of electron transition in the material. n is equal to 2 or 1/2 for indirect and direct transition band respectively (Jubu et al., 2020). Commonly, the band gap energy of materials is estimated from the diffuse reflectance spectra following Kubelka-Munk (K-M) theory (Džimbeg-Malčić et al., 2011). In the K-M theory, the reflectance data can be converted into absorption spectra by applying Eq. (7)

$$F(R) = \frac{(1-R)^2}{2R} = \frac{K}{S} \quad (7)$$

where F(R) is the K-M function, R is the diffuse reflectance, K is absorption coefficient and S is a scattering coefficient. Substituting F(R) for α in Eq. (6) gives a modified Tauc expression Eq. (8)

$$(F(R)h\nu)^{1/n} = C(h\nu - E_g) \quad (8)$$

Putting n equal to 1/2 for a direct electron band transition in In_2O_3, Figure 6 (b) shows a plot of $(F(R)hν)^2$ against the incident photon energy (hν) according to Eq. (8) for which the horizontal axis intercept of the linear fit of the Tauc plot gives approximate values for the band gap energies of the In_2O_3 films synthesized at various deposition temperatures. Band gap values of 3.470, 3.279, 3.021, and 3.044 eV were obtained respectively for the films grown at 850, 900, 950, and 1000 ^oC.

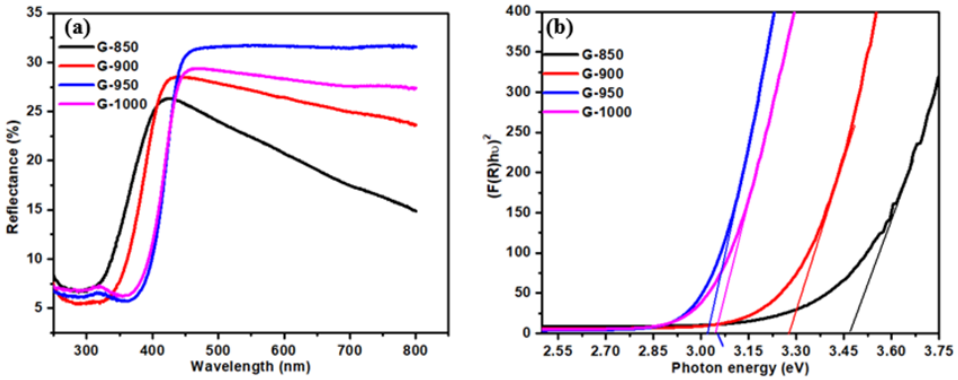

Figure 6 : (a) Reflectance Spectra for the In_2O_3 Films Synthesized at Different Temperatures, (b) Tauc Plot showing Bandgap Energy for the In_2O_3 films Synthesized at Different Temperatures

CONCLUSION

In this study, indium oxide (In_2O_3) thin films were successfully deposited on glass substrates using the chemical vapour deposition (CVD) technique by carefully controlling the deposition conditions. The effect of source temperature on the growth and properties of the films was systematically investigated within the temperature range of 850 °C to 1000 °C. The results showed that deposition temperature strongly influences the morphology, crystallinity, and optical behaviour of the synthesized films.

Morphological analysis revealed the evolution of distinct microstructures with varying geometries and grain distributions as the growth temperature increased, indicating temperature-dependent nucleation and growth mechanisms. Structural characterization confirmed the formation of highly crystalline body-centered cubic (BCC) In_2O_3 films with a preferred orientation along the (222) plane, demonstrating improved crystalline quality at elevated temperatures. Optical studies showed that the films possess low reflectance characteristics and exhibited a progressive narrowing of the optical bandgap from 3.470 eV to 3.021 eV with increasing deposition temperature.

The successful deposition of crystalline In_2O_3 thin films on ordinary glass substrates highlights the potential of the CVD technique for producing cost-effective transparent oxide materials without the need for expensive high-temperature-resistant substrates such as sapphire or quartz. The tunable optical and structural properties obtained in this work suggest that these films are promising candidates for applications in optoelectronic devices, transparent conductive coatings, solar cells, and sensing technologies. Furthermore, the study provides useful insight into the optimization of growth parameters for tailoring the performance of In_2O_3 thin films for specific advanced technological applications.

ACKNOWLEDGMENT

Aper sincerely appreciate the School of Physics, Universiti Sains, Malaysia for providing all of the laboratory facilities for this research work. The authors thank Rev. Fr. Moses Orshio Adasu, University (formally Benue State University), Makurdi, Nigeria for providing the enabling environment.

REFERENCE

Ahmed, N. M., Sabah, F. A., Abdulgafour, H. I., Alsadig, A., Sulieman, A., & Alkhoaryef, M. (2019). The effect of post annealing temperature on grain size of indium-tin-oxide for optical and electrical properties improvement. *Results in Physics*, *13*(February), 102159. https://doi.org/10.1016/j.rinp.2019.102159

Aper, T M, Yam, F. K., Saw, K. G., Poay, K., & Chahrour, K. M. (2021). Results in Physics Atmospheric pressure chemical vapor deposition of indium oxide nanostructured films for photoelectrochemical application. *Results in Physics*, *24*(April), 104187. https://doi.org/10.1016/j.rinp.2021.104187

Aper, T Moses, Tyona, M. D., Yam, F. K., & Beh, K. P. (2023). *Structural and Optical Characterization of Electrochemically Deposited Indium Oxide Nanostructures for Photoelectrochemical Investigation*. https://doi.org/10.1021/acs.cgd.2c01185

Domènech-Gil, G., Barth, S., Samà, J., Pellegrino, P., Gràcia, I., Cané, C., & Romano-Rodriguez, A. (2017). Gas sensors based on individual indium oxide nanowire. *Sensors and Actuators, B: Chemical*, *238*, 447–454. https://doi.org/10.1016/j.snb.2016.07.084

Džimbeg-Malčić, V., Barbarić-Mikočević, Ž., & Itrić, K. (2011). Kubelka-Munk theory in describing optical properties of paper (I). *Tehnički Vjesnik : Znanstveno-Stručni Časopis Tehničkih Fakulteta Sveučilišta u Osijeku*, *18*(1), 117–124.

Elam, J. W., Martinson, A. B. F., Pellin, M. J., & Hupp, J. T. (2006). Atomic layer deposition of in 2O 3 using cyclopentadienyl indium: A new synthetic route to transparent conducting oxide films. *Chemistry of Materials*, *18*(15), 3571–3578. https://doi.org/10.1021/cm060754y

Gan, J., Lu, X., Wu, J., Xie, S., Zhai, T., Yu, M., Zhang, Z., Mao, Y., Wang, S. C. I., Shen, Y., & Tong, Y. (2013). Oxygen vacancies promoting photoelectrochemical performance of in 2 O 3 nanocubes. *Scientific Reports*, *3*, 1–7. https://doi.org/10.1038/srep01021

Her, S.-C., & Chang, C.-F. (2017). Fabrication and characterization of indium tin oxide films. *Journal of Applied Biomaterials & Functional Materials*, *15*(2), 0–0. https://doi.org/10.5301/jabfm.5000345

Hosseini, a, Icli, K. C., & Güllü, H. H. (2013). Preparation and characterization of porous TiO 2 thin films by sol-gel method for Extremely Thin Absorber-ETA solar cell applications Çok ince Soğurucu – ETA g üneş gö zeler e uygulamaları için gö zenekli TiO 2 ince filmlerin sol-jel metodu ile ü retilmes. *Turkish Journal of Science & Technology*, *8*(2), 69–79.

Jubu, P. R., Aper, T. M., & Igba, V. M. (n.d.). *Growth Mechanism and Structural Elucidation of Indium Oxide Microstructures Prepared by Carbothermal and Hydrogen Reduction Processes*.

Jubu, P. R., Yam, F. K., & Moses, A. T. (2020). Deposition of Gallium Oxide Nanostructures at Low Substrate Temperature by Chemical Vapor Deposition. *ECS Journal of Solid State Science and Technology*, *9*(3), 035006. https://doi.org/10.1149/2162-8777/ab7b47

Karazhanov, S. Z., Ravindran, P., Vajeeston, P., Ulyashin, A., Finstad, T. G., & Fjellvåg, H. (2007). Phase stability, electronic structure, and optical properties of indium oxide polytypes. *Physical Review B - Condensed Matter and Materials Physics*, *76*(7), 1–13. https://doi.org/10.1103/PhysRevB.76.075129

Karn, A., Kumar, N., & Aravindan, S. (2017). Chemical vapor deposition synthesis of novel indium oxide nanostructures in strongly reducing growth ambient. *Journal of Nanostructures*, *7*(1), 64–76. https://doi.org/10.22052/jns.2017.01.008

King, P. D. C., Veal, T. D., Fuchs, F., Wang, C. Y., Payne, D. J., Bourlange, A., Zhang, H., Bell, G. R., Cimalla, V., Ambacher, O., Egdell, R. G., Bechstedt, F., & McConville, C. F. (2009). Band gap, electronic structure, and surface electron accumulation of cubic and rhombohedral In2 O3. *Physical Review B - Condensed Matter and Materials Physics*, *79*(20), 1–10. https://doi.org/10.1103/PhysRevB.79.205211

Lei, F., Sun, Y., Liu, K., Gao, S., Liang, L., Pan, B., & Xie, Y. (2014a). Oxygen vacancies confined in ultrathin indium oxide porous sheets for promoted visible-light water splitting. *Journal of the American Chemical Society*, *136*(19), 6826–6829. https://doi.org/10.1021/ja501866r

Lei, F., Sun, Y., Liu, K., Gao, S., Liang, L., Pan, B., & Xie, Y. (2014b). Oxygen vacancies confined in ultrathin indium oxide porous sheets for promoted visible-light water splitting. *Journal of the American Chemical Society*, *136*(19), 6826–6829. https://doi.org/10.1021/ja501866r

Li, C., Zhang, D., Han, S., Liu, X., Tang, T., Lei, B., Liu, Z., & Zhou, C. (2003). Synthesis, Electronic Properties, and Applications of Indium Oxide Nanowires. *Annals of the New York Academy of Sciences*, *1006*(2), 104–121. https://doi.org/10.1196/annals.1292.007

Li, Chao, Zhang, D., Liu, X., Han, S., Tang, T., Han, J., & Zhou, C. (2003). In2O3 nanowires as chemical sensors. *Applied Physics Letters*, *82*(10), 1613–1615. https://doi.org/10.1063/1.1559438

Li, Conan, & Han, S. (2003). *Ultraviolet photodetection properties of indium oxide nanowires*. *January 2016*. https://doi.org/10.1007/s00339-003-2099-3

Liang, C. H., Meng, G. W., Lei, Y., Phillipp, F., & Zhang, L. D. (2001). Catalytic growth of semiconducting In2O3 nanofibers. *Advanced Materials*, *13*(17), 1330–1333. https://doi.org/10.1002/1521-4095(200109)13:17<1330::AID-ADMA1330>3.0.CO;2-6

Ma, Q., Zheng, H. M., Shao, Y., Zhu, B., Liu, W. J., Ding, S. J., & Zhang, D. W. (2018). Atomic-Layer-Deposition of Indium Oxide Nano-films for Thin-Film Transistors. *Nanoscale Research Letters*, *13*(1). https://doi.org/10.1186/s11671-017-2414-0

Mahalingam, S., & Abdullah, H. (2016). Electron transport study of indium oxide as photoanode in DSSCs: A review. *Renewable and Sustainable Energy Reviews*, *63*, 245–255. https://doi.org/10.1016/j.rser.2016.05.067

Piper, L. F. J., Demasi, A., Cho, S. W., Smith, K. E., Fuchs, F., Bechstedt, F., Körber, C., Klein, A., Payne, D. J., & Egdell, R. G. (2009). Electronic structure of In2 O3 from resonant x-ray emission spectroscopy. *Applied Physics Letters*, *94*(2), 1–4. https://doi.org/10.1063/1.3070524

Qurashi, A., Irfan, M. F., & Alam, M. W. (2010). In2O3 nanostructures and their chemical and biosensor applications. *Arabian Journal for Science and Engineering*, *35*(1 C), 125–145.

Ray, S., Banerjee, R., Basu, N., Batabyal, A. K., & Barua, A. K. (1983). Properties of tin doped indium oxide thin films prepared by magnetron sputtering. *Journal of Applied Physics*, *54*(6), 3497–3501. https://doi.org/10.1063/1.332415

Sakaliuniene, J., Čyviene, J., Abakevičiene, B., & Dudonis, J. (2011). Investigation of structural and optical properties of GDC thin films deposited by reactive magnetron sputtering. *Acta Physica Polonica A*, *120*(1), 63–65. https://doi.org/10.12693/APhysPolA.120.63

Stroescu, H., Anastasescu, M., Preda, S., Nicolescu, M., Stoica, M., Stefan, N., Kampylafka, V., Aperathitis, E., Modreanu, M., Zaharescu, M., & Gartner, M. (2013). Influence of thermal treatment in N2 atmosphere on chemical, microstructural and optical properties of indium tin oxide and nitrogen doped indium tin oxide rf-sputtered thin films. *Thin Solid Films*, *541*(February), 121–126. https://doi.org/10.1016/j.tsf.2012.11.135

Yahia, A., Attaf, A., Saidi, H., Dahnoun, M., Khelifi, C., Bouhdjer, A., Saadi, A., & Ezzaouia, H. (2019). Structural, optical, morphological and electrical properties of indium oxide thin films prepared by sol gel spin coating process. *Surfaces and Interfaces*, *14*(October 2018), 158–165. https://doi.org/10.1016/j.surfin.2018.12.012

Zhang, Q., Wang, S., Fu, H., Wang, Y., Yu, K., & Wang, L. (2020). *Facile Design and Hydrothermal Synthesis of In 2 O 3 Nanocube Polycrystals with Superior Triethylamine Sensing Properties*. https://doi.org/10.1021/acsomega.0c00497